Precision Stark spectroscopy of sodium: Improved values for the ionization limit and bound states

M. Ciocca, C. E. Burkhardt, and J. J. Leventhal
University of Missouri–St. Louis, St. Louis, Missouri 63121

T. Bergeman
State University of New York at Stony Brook, Stony Brook, New York 11794
(Received 16 August 1991; revised manuscript received 15 November 1991)

We report results of a combined theoretical and experimental investigation that uses Stark spectroscopy of high-lying Rydberg states to measure accurately zero-field atomic parameters. Improved values for the binding energies of the 11 ^2S, 12 ^2S, and 10^2D states of sodium are presented. These results are combined with previous data in a global least-squares fit to obtain improved quantum-defect parameters for the sodium ^2S and ^2D manifolds. Using previous precision optical data, the present results, and the quantum-defect expansion, we obtain an improved value for the ionization limit of neutral sodium: $E_{\rm ion}=41\,449.451(2)$ cm^{-1}. The consequences of the improved ionization energy on the quantum-defect expansion parameters of the ^2P states are also discussed and values are obtained from fits to the available data.

PACS number(s): 32.30.Bv, 35.10.Hn, 32.60.+i, 32.80.Rm

I. INTRODUCTION

The pioneering experiments of Stark [1] and LoSurdo [2] in the early part of this century provided the basis for the use of stark spectroscopy for studying atomic properties. There have been numerous investigations of Stark-level structure in hydrogen, helium, alkali-metal and other atoms since these first observations. Most relevant for our present purposes are the landmark studies by Kleppner and co-workers [3] in which tunable dye-laser excitation was used to observe the structure of alkali-metal atoms with principal quantum number near 15 in an electric field F. The observed pattern of energy levels up to the saddle point $E=-2\sqrt{F}$ agreed well with calculations using a basis of spherical states shifted at zero field in accord with well-known quantum-defect (QD) parameters.

In this paper we present results of a combined theoretical and experimental study of high-lying Rydberg states of sodium (in the range $n=34$–65) in electric fields below 20 V/cm. The Stark-level structure is, however, of secondary interest; our primary objective is to use calculated Stark shifts to improve our knowledge of zero-field energies. Also, in contrast to the more usual procedure, we scan the electric field at fixed laser frequency. Extremely high resolution is obtained by using a line-selectable CO_2 laser as the final step of a three-laser excitation sequence. The spectra of excited atoms versus electric field are matched with results of theoretical calculations using matrix diagonalization over a basis of spherical coordinate wave functions, as in Ref. [3]. From this comparison, we obtain the energy of the upper state excited by the CO_2 laser by least-squares fit. Then, using the accurate values for the CO_2-laser line energies, we obtain improved values for the binding energies of the lower states of the CO_2-laser transition.

In applying this method, we have subjected our computed Stark energy-level structure to stringent tests to examine the effect of uncertainties in the input QD parameters, the accuracy of numerically computed wave functions, and the size of the basis set of zero-field levels. Martin [4] has published a thorough review and analysis of sodium Rydberg-series parameters, and we have performed our own weighted least-squares fits to incorporate data obtained since this review, including the present results used iteratively. Because most of the basis states for these high-n Rydberg levels are very nearly hydrogenic, the uncertainty in the QD parameters affects the results less than other uncertainties in the data analysis. Also, by comparison with analytic formulas for dipole matrix elements in the limit of zero QD (nonrelativistic hydrogen), we verify that our numerically computed wave functions are accurate to the precision required. The effect of the size of the basis set used in the Stark-level calculations has been more troublesome because of the relatively slow convergence as additional n levels are added, and the size of the matrices required by Rydberg structures above $n=30$. These factors will be discussed further in Sec. III.

Although sodium is one of the most extensively studied atoms, there do not exist the extensive precision Doppler-free laser spectroscopic measurements on many Rydberg levels such as one has for heavier alkali metals [5–7]. Thus, the precise knowledge of sodium energy levels obtained from microwave (MW) spectroscopy on levels above $n=16$ [8–11] has not led to comparably precise binding energies and series formulas for lower levels. Our data on intermediate Rydberg levels help to fill this gap. For example, our term value for the 10^2D state removes the large discrepancy ($\sim$0.08 cm^{-1}) noted in fits [4,12] to the earlier data. Improved values for the sodium QD parameters are thereby obtained (Sec. IV), leading to improved values for all ^2S and ^2D state energies. The fitted term values and QD parameters together with

previous interferometric measurements [13,14] are then used to obtain an improved value for E_{ion}, the ionization potential of ground-state sodium atoms (Sec. V). Finally, using this value for E_{ion} and available spectroscopic data, we discuss and present QD parameters for ^2P, ^2F, and higher-L states (Sec. VI).

II. EXPERIMENT

The experiments were conducted using an atomic-beam apparatus and three-photon absorption, from three different laser beams, to excite sequentially ground-state sodium atoms. The sodium beam was produced in an effusive oven located 5 cm below a stainless-steel cell within which the atomic excitation occurs at the intersection of the laser beams with the atomic beam [15]. The density of the atomic beam was typically 10^7 cm^{-3}, as measured by a method previously discussed [16].

The excitation scheme for these experiments is illustrated in Fig. 1 for the case in which $12\,^2S$ is the second intermediate state. Two visible laser beams, one yellow and the other blue, produced by grazing-incidence dye lasers pumped by a single pulsed Nd:YAG (where YAG stands for yttrium aluminum garnet) laser were used to excite sequentially $3\,^2S \rightarrow 3\,^2P \rightarrow 12\,^2S$. The pulse length was ~7 nsec with a 10-Hz repetition rate. The final step in the sequence was effected with a cw CO_2 laser equipped with a grating for line selectivity, thus permitting the use of all lines of the 9- and 10-μm P and R branches spanning the energy range 950–1050 cm^{-1}. A piezoelectric-controlled output mirror was used to scan the laser frequency within the gain curve of a given molecular transition.

The experimental configuration of laser beams, atomic beams, and electrostatic field is shown schematically in Fig. 2. The stainless-steel interaction cell (not shown in the figure) serves as an electrostatic shield and is equipped with a pair of parallel plates between which an electric field may be applied. This field was set to the desired value for a particular data point prior to the laser pulses, but was increased about 1 μsec after the pulses to a value, 20–50 V/cm, sufficient to ionize the highly excited atoms. Because high-lying Rydberg states were under study, only modest voltages were required to produce the necessary fields. The signal generator was therefore

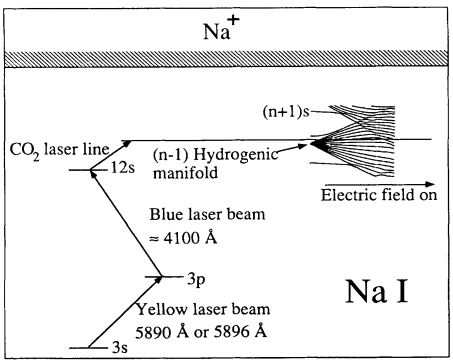

FIG. 1. Partial energy-level diagram of sodium illustrating the excitation sequence employed in these experiments.

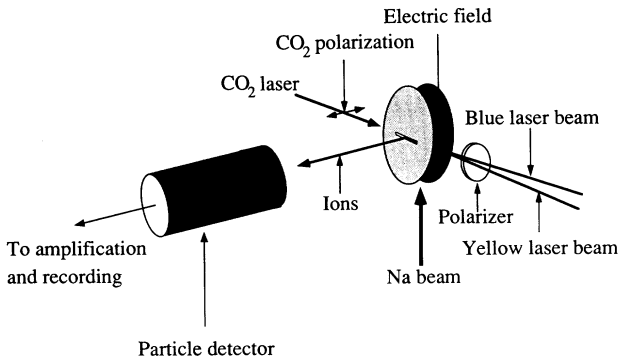

FIG. 2. Schematic diagram of the apparatus.

powered by batteries to minimize ground-loop effects. Detection of an ion after the final field pulse served to indicate that an atom had absorbed all three photons.

After formation in the interaction region, ions were electrostatically focused and detected with a CuBe particle-multiplier tube, the output of which was fed into a charge-sensitive amplifier. Stark spectra were acquired with all three laser wavelengths fixed. The visible lasers were tuned to produce a particular (second) intermediate state, $11\,^2S$, $12\,^2S$, or $10\,^2D$, while the Stark field was scanned stepwise over the range of interest. These Stark spectra thus consist of ion signal versus electric field. The parallel plates inside the interaction cell were designed to produce a uniform field and to minimize field inhomogenities that could distort the Stark spectrum. We therefore made the plates as large as possible, 7.5 cm in diameter, and used a slit 2.5 cm long by 500 μm wide in accordance with the design scheme developed at Stony Brook [17,18]. Symmetric scans of the electric field, positive to negative, were used to minimize the offset of the nominal zero-field value. In addition to parallelism of the plates, it was found that the location of the interaction volume, defined by the intersection of the laser beams with the atomic beam, had a profound effect on the offset. As might be expected, when this volume was placed at the midpoint between the plates the offset was minimized. Moreover, it was found that the offset could be further reduced by symmetrically scanning the voltage applied to each plate, one toward higher voltage and the other toward lower, rather than fixing the voltage on one plate while scanning the voltage on the other. This procedure maintained the midpoint between the plates at earth ground, the same potential as that of the interaction cell. By these means we were able to reduce the electric-field offset to less than 80 mV/cm, as determined from fits to the data as discussed below.

In fitting the data to the theoretical energy levels, in addition to the field-offset parameter to provide an adjustable shift in the effective-field zero value, we used also a field-calibration factor to adjust the effective plate spacing. The calibration factor relative to the nominal value for a plate spacing of 1.11(5) cm varied between 0.989(3) and 0.997(3) in different runs, presumably depending on the position of the interaction region relative to the aperture in the field plates required for extracting the ions.

The CO_2 transition frequencies have been measured

[19] to 10^{-8} cm^{-1} and are conveniently tabulated in Ref. [20]. According to Ref. [21], pressure shifts are negligible if the cavity is adjusted to optimum, while discharge current shifts are less than 10 MHz. Hence in the data analysis below, we are able to quote binding energies of the 11 and 12 ^2S and 10 ^2D states to estimated errors of this magnitude.

III. RESULTS

The interplay between experiment and theory is demonstrated by comparing the positions of the peaks in an experimental spectrum with calculated Stark energies. The correspondence is conveniently illustrated by placing the recorded spectrum on a map of Stark energies versus electric field at the energy obtained from our fitting procedure. Figure 3 is a particularly simple example. In this case, the $3\,^2P_{3/2}$ and the $11\,^2S$ state were excited by the dye lasers; the 9 $R(28)$ line of the CO_2 laser was used for the final step in the sequence. The top half of Fig. 3 shows the observed peaks versus electric field. Since the CO_2 laser was polarized parallel to the static electric field, only $|m_j|=1/2$ levels of the final-state manifold were (in principle) excited. The lower half of the figure shows calculated energies of $|m_j|=1/2$ Stark levels emanating from $n=34$, up to the fitted excitation energy. The procedure for computing the Stark energies is discussed below. When the fine-structure mixing is not large, as is usually the case in sodium, the $|m_j|=1/2$ states are quite pure $m_l=0$ or $|m_l|=1$. (There are regions where mixing is significant.) For π-polarized laser light from a lower S state, only states with large $m_l=0$ character are excited, so typically only one of each doublet pair of levels has appreciable intensity. Theoretically computed intensities were used to indicate which component should be fitted to the observed peak position. The theoretical and experimental intensities did not, however, agree quantitatively because of departures from ideal polarization and pulse-to-pulse variation of the laser intensity.

From this particular data scan and the theoretical Stark energies, it was possible to fit just two parameters,

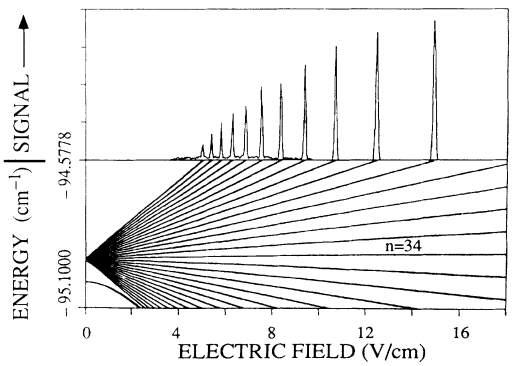

FIG. 3. Observed peaks in a scan over electric field (top half) when the 9 $R(28)$ CO_2-laser line interacts with the 11 ^2S state. The bottom half shows Stark energies from the $n=34$ manifold, including the 34 ^2D state, up to the fitted upper-level energy of -94.5773 cm^{-1}.

the excitation energy and the field offset. The quoted error limits on the excitation energy must therefore reflect also the range of possible values for the calibration factor cited above. In other cases, the calibration factor could be fit from the data. Tables I–III present the fitting procedure more explicitly. Table I gives peak positions fitted to the data of Fig. 3. Peak positions fitted to the field-scan data (column 1) are fitted to theoretical energies for levels found to have predominantly $m_l=0$ character. The adjusted peak positions (column 2), obtained by taking into account the fitted field offset and assumed calibration factor, exhibit an rms discrepancy with calculated values of about 2 mV/cm (column 3), as compared with typically 1 mV/cm uncertainties in the peak positions (column 4). The parameters from this fit, as well as the fit for the data in Table II, are given in Table III. The probable range of the calibration factor introduces uncertainty limits in the upper-level energy of 0.0027 cm^{-1} for the data of Table I. (All error limits quoted in this paper correspond to one standard deviation.)

Table II and Fig. 4 show results of a field scan that is much more sensitive to the value of the excited-state energy than the data of Table I and Fig. 3 and is correspondingly more complicated. For this scan, the $3\,^2P_{1/2}$ state and the $12\,^2S$ state were the intermediate states. The 10 $P(44)$ line of the CO_2 laser, again polarized parallel to the static electric field, provided the final excitation step. Plotted in the upper half of Fig. 4 are the $|m_j|=1/2$ energy levels emanating from $n=49$ and from the $50\,^2S$ level at -46.3599 cm^{-1}, up to the region [17,3], where there are many anticrossings between levels from adjacent n manifolds. Because of the differing slopes of the various components, it was possible in this case to fit

TABLE I. Measurements and results of a least-squares fit to peaks in the electric-field scan for the excitation of $11\,^2S$ by the CO_2 9 $R(28)$ line, as shown in Fig. 3. Column 1 gives results of a fit to the digitized field-scan data. Column 2 gives the peak position after correction by the assumed calibration factor and fitted offset. Column 3 is the difference in the calculated and corrected peak positions. Column 4 is the standard deviation from the fit to the individual peaks. The observed peaks correspond to transitions to predominantly $m_l=0$ sublevels among the $|m_j|=1/2$ manifold. When the lower state is an S state and the CO_2 laser is polarized parallel to the electric field, transitions to $|m_l|=1$ sublevels have negligible intensity and are therefore omitted.

Measured (V/cm)	Corrected (V/cm)	Discrepancy (mV/cm)	Expt. std. dev. (mV/cm)
5.0780	4.9834	2.4	5.1
5.4554	5.3583	−1.8	1.0
5.8733	5.7732	0.4	1.4
6.3567	6.2532	1.6	1.0
6.9288	6.8213	−1.8	1.5
7.6054	4.4932	0.7	1.6
8.4344	8.3164	−1.7	1.4
9.4629	9.3577	−0.1	0.7
10.7792	10.6448	4.8	1.1
12.5444	12.3976	−0.2	0.5
15.0143	14.8502	−2.5	1.4

TABLE II. Results of a least-squares fit to peaks in the electric-field scan for the excitation of $12\,^2S$ by the CO_2 9 $P(44)$ line. Column 1 gives results of a fit to the digitized field-scan data. Column 2 gives the peak position after correction by the assumed calibration factor and fitted offset. Column 3 is the difference between the corrected peak and the value calculated at the fitted energy. Column 4 is the standard deviation from the fit to the individual peaks. As in Table I, only predominantly $m_l=0$ sublevels are included in this listing.

Measured (V/cm)	Corrected (V/cm)	Discrepancy (mV/cm)	Expt. std. dev. (mV/cm)
4.5119	4.3983	−2.5	0.5
4.7710	4.6550	3.1	0.3
4.9994	4.8813	4.4	0.3
5.2241	5.1237	1.9	0.5
5.5246	5.4016	−7.3	0.3
5.8205	5.6948	−3.0	0.5
6.1561	6.0272	−3.6	0.3
6.5311	6.3988	−0.4	0.6
6.9621	6.8258	0.7	0.4
7.4553	7.3145	4.0	0.5
8.0378	7.8916	5.7	0.6
8.7828	8.6296	−0.3	1.1
9.8778	9.7146	−0.9	1.0

a calibration factor as well as the field-offset parameter and upper-level energy (see Table III). Even though, as shown in Table II, the agreement between theoretical and observed peaks for these data exhibits an rms deviation of about 4 mV/cm (as compared with measuring uncertainties of ≤ 1 mV/cm), it was nevertheless possible to determine the excitation energy to essentially the width of the CO_2 laser line itself.

When the second intermediate state was the $10\,^2D_{5/2}$ state and either of the dye lasers contained some polarization perpendicular to the electric field, $|m_j|=3/2$ and 5/2 final-state levels could be excited. An example of this is shown in Fig. 5, which contains a spectrum obtained when the $3\,^2P_{3/2}$ level, the first intermediate level, and the 9 $P(20)$ CO_2 laser line were used. In the bottom half of the figure are levels emanating from $n=45$. Energies for $|m_j|=1/2$ (solid lines) and $|m_j|=3/2$ (dashed lines) are shown. Clearly, some of the experimental peaks correspond to $|m_j|=3/2$ levels due to imperfect polarization. Because of possible unresolved overlaps with $|m_j|=5/2$ levels, parameters derived from this particular scan are not used in the following discussion.

TABLE III. Fit parameters for the field-scan data in Tables I and II.

Parameters for 9 $R(28)$ on $11\,^2S$		
Assumed calibration constant	0.989	0.997
Fitted offset	−0.053(2) V/cm	−0.056(2) V/cm
Fitted upper-level energy	−94.5791(7) cm^{-1}	-94.5764(7) cm^{-1}
Parameters for 9 $P(44)$ on $12\,^2S$		
Fitted calibration constant	0.9900(14)	
Fitted offset	−0.065(4) V/cm	
Fitted upper-level energy	−46.3859(4) cm^{-1}	

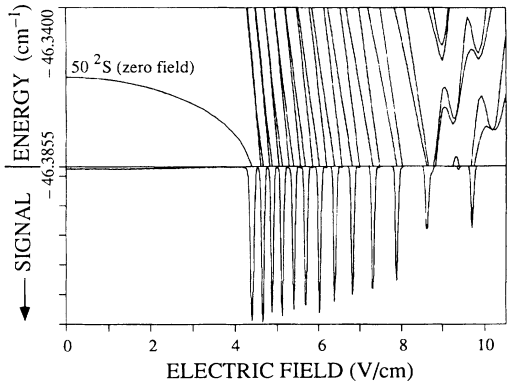

FIG. 4. Observed peaks in a scan over electric field (bottom half) when the 10 $P(44)$ CO_2 laser line interacts with the $12\,^2S$ state. The top half shows levels shifted downwards from $n=49$ and the $50\,^2S$ state, and some levels shifted upwards from $n=48$ in the region just above the fitted upper-level energy of $-46.3859\ cm^{-1}$.

The evaluation of uncertainties for the energies quoted here also involves uncertainties in the theoretical Stark energies. This includes the question of the numerical accuracy of the wave functions and the dipole elements and then the reliability of the zero-field energies obtained from QD theory. According to the Coulomb approximation, wave functions for the n, J, L spherical-coordinate basis states are computed by inward integration from infinity at the appropriate zero-field energy [3]. Our radial wave functions were computed with a $\sqrt{r}$ scaling so that a nearly equal number of mesh points occur between nodes [22]. The accuracy of these wave functions was checked by comparing computed dipole moments with analytic formulas in the limit of zero QD. In every case examined, there was agreement to better than 1 part in

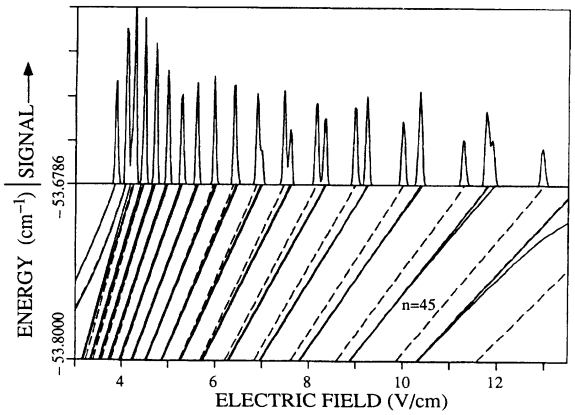

FIG. 5. Observed peaks in a scan over electric field (top half) from sequential excitation of the $3\,^2P_{3/2}$ and $10\,^2D_{5/2}$ states, followed by interaction with the 9 $P(20)$ CO_2 laser line. The bottom half shows $|m_j|=1/2$ levels (solid lines) and $|m_j|=3/2$ levels (dashed lines) emanating from $n=45$ up to the fitted upper-level energy.

10^6, so that calculated Stark shifts of 10 cm^{-1} (more than occurs here) may be considered accurate to 10^{-5} cm^{-1}.

The number of basis states required to achieve energy convergence was determined by progressively adding one n level above and one below. For higher n and for scans to higher values of the field, more basis states were required. For each data set, convergence to 1×10^{-4} cm^{-1}, or to a small fraction of the other uncertainties, was attained. For $|m_j|=1/2$, each n manifold involves $2n-1$ basis states.

Quantum-defect expansions for the important low-L manifolds are obtained from empirical analysis of available data. Martin's parameters [4] are based on data published prior to 1980. We have fit parameters using subsequent data and also the present results. In turn, fits were made with Stark levels calculated with the updated parameters (see Secs. IV and VI) iterated to self-consistency. The difference in results obtained with our QD expansions and those in Ref. [4] ranged from 2×10^{-6} to 8×10^{-5} cm^{-1}. When the fitted QD parameters were varied over their uncertainty limits the effects were also less than 1×10^{-4} cm^{-1}. A variation of 3% in the dipole polarizability (see Sec. VI), corresponding to the uncertainty suggested in Ref. [23], in one case [9 $P(44)$ on 12 ^2S] did produce a change of 1.5×10^{-4} cm^{-1}, but less for the other CO_2 line excitations studied. We conclude that the effect of uncertainties in the Rydberg-state energies adds only marginally to the quoted error limits, in quadrature. The reason for this small variation lies in the high degree of precision with which the Rydberg states of sodium have been determined, and also in the fact that for $n\geq34$, most of the sodium levels are effectively hydrogenic.

Table IV presents the data for two transitions each for CO_2-laser excitations from the 11 ^2S, 12 ^2S, and 10 ^2D intermediate states. The n manifolds included in the basis set for the Stark-structure calculations are given in column 4. The largest basis set, for line 5, included 801 n,L,J states. The basis sets indicated in line 4 and 6 of this table are smaller than the others because the maximum electric field at which peaks were recorded in these cases was less than 5 V/cm, compared with 10–17 V/cm in the other case. The "fitted upper-level energy" values quoted in column 5 were obtained by iteration such that the experimental data were eventually compared with Stark-level energies computed with final converged QD values reported in Secs. IV and VI. For each of the lower states, the binding energy (energy relative to the zero-field threshold) is determined by adding the fitted Stark-shifted upper-state energies and the CO_2-laser wave number.

The cases for which larger error limits quoted in Table IV are those for which the field calibration factor could not be fitted from the data itself, but was introduced as a parameter varying between 0.989 and 0.997. The data obtained with the 9 $R(26)$ CO_2 laser line exciting the 11 ^2S state happened to include just six nearly equidistant peaks over the range from 11 to 18 V/cm. Hence the fitted upper-level energy for this line was particularly sensitive to the assumed calibration factor, resulting in larger error limits than for the other cases. The term value for 11 ^2S is therefore determined primarily by the data obtained with 9 $R(28)$, and similarly for 12 ^2S, the value with 10 $P(44)$ predominates. As shown in Table V, the weighted-average ^2S-state results are consistent with previous determinations [12], but are about 20 to 150 times more accurate. For the 10 ^2D state, the previous measurement is seen to be in error by 0.08 cm^{-1}, as was noted already in fitting the ^2D-state term values [12,4], so the new energy value removes this discrepancy and represents an improvement by a factor of ~200.

It may be noted from Table IV that the difference in fitted upper-state energy for the two cases (lines 5 and 6) in which 10 ^2D levels were excited by CO_2 laser lines reflects the $10\,^2D_{5/2}-10\,^2D_{3/2}$ splitting. Our results confirm that the 10 ^2D state is inverted, and the splitting we obtain, 78(36) MHz, is within error limits of the much more accurate value, 91.5±1.0 MHz, from quantum-beat spectroscopy [24]. The 10 ^2D-state energy quoted in Table V is primarily from 9 $P(26)$ excitation of $10\,^2D_{5/2}$ and uses the quantum-beat determination of the fine-structure splitting to obtain the ^2D state center of gravity.

IV. QD PARAMETERS FOR SODIUM ^2S AND ^2D STATES

Since the last review of sodium series formulas by Martin [4], there have been improved measurements of the D lines [13] ($3\,^2S\rightarrow3\,^2P_{1/2}$ and $^2P_{3/2}$), and improved microwave measurements [8] as well as the present results.

TABLE IV. This table gives the intermediate sodium atomic level that is the lower level for the CO_2 laser transition, the CO_2 laser wave number, the n range of the n,L,J basis states used in the Stark-level calculation, the fitted upper-state binding energy, and the binding energy of the lower level, obtained by adding the previous two figures. Predominantly, even in electric fields of interest here, $^2D_{3/2}$ is excited from $3\,^2P_{1/2}$, and $^2D_{5/2}$ from $3\,^2P_{3/2}$.

Atomic level	CO_2 laser Line	CO_2 laser Energy[a] (cm^{-1})	Basis states n	Fitted upper-level energy (cm^{-1})	Lower-level energy (cm^{-1})
11 ^2S	9 $R(26)$	1082.2962	30–38	−95.7563(33)	−1178.0525(33)
11 ^2S	9 $R(28)$	1083.4788	30–38	−94.5777(14)	−1178.0565(14)
12 ^2S	10 $P(38)$	927.0083	49–55	−40.2080(15)	−967.2163(15)
12 ^2S	10 $P(44)$	920.8291	45–52	−46.3859(4)	−967.2150(4)
$10\,^2D_{3/2}$	9 $P(20)$	1046.8542	41–49	−53.6777(9)	−1100.5319(9)
$10\,^2D_{5/2}$	9 $P(26)$	1041.2791	41–45	−59.2554(4)	−1100.5345(4)

[a]Reference [20].

TABLE V. A comparison of the weighted-average term values of the intermediate sodium atomic level with previous experimental determinations and the value calculated from the QD parameters obtained by fitting all available data (including data presented here) with appropriate weights. Columns 2–4 give the binding energy, while column 5 gives the energy relative to Na $3\,^2S$, taking the ionization energy to be 41 449.451(2) cm^{-1}. The ^2D figures are for the center of gravity of the fine-structure components.

Atomic level	Previous term value[a] (cm^{-1})	Weighted average (cm^{-1})	From fitted QD params. (cm^{-1})	Energy rel. to Na $3\,^2S$ (cm^{-1})
$11\,^2S$	−1178.06(3)	−1178.0555(15)	−1178.0554	40271.396(2)
$12\,^2S$	−967.22(3)	−967.2151(4)	−967.2152	40482.236(2)
$10\,^2D$	−1100.61(3)	−1100.5328(4)	−1100.5328	40348.918(2)

[a]References [12,25].

It is therefore appropriate to reconsider the series formulas for the ^2S and ^2D manifolds. The QD parameters are useful in any calculation of sodium Rydberg-level energies and in particular in the estimation of the ionization energy as in the following section.

Table VI presents the available data for sodium ^2S states. Intervals from $3\,^2S$ to $N=4-12\,^2S$ are obtained from the very precise D-line data of Juncar *et al.* [13] plus $n\,^2S\rightarrow 3\,^2P$ transitions measured by Meissner and Luft [14] (for $n=5$, 6, and 7) or by Risberg [12] for $n=4$ and $n=8-12$. The Meissner and Luft [14] measurements were quoted to an accuracy of 5×10^{-5} nm, which translates to 8×10^{-4} cm^{-1} for the $5\,^2S$ energy and 2.2×10^{-3} cm^{-1} for $7\,^2S$. As Martin and Zalubas [25] have noted, however, the Kr line used as a standard has been redetermined, so that all wavelengths reported by Meissner and Luft should be increased by 7 parts in 10^8. With this correction, the D-line measurements of Meissner and Luft are confirmed by Juncar *et al.* [13] to well within their quoted error limits. We therefore conclude that the other transitions measured by Meissner and Luft are valid to the stated precision after correcting for the revised Kr standard. The intervals from $n\rightarrow n+1$ for $n\geq 32$ are from two-photon microwave measurements of very high precision [8].

We have utilized the experimental intervals listed in Table VI in a global least-squares fit to QD parameters. Appropriate weights reflect the accuracy of each data point. Energies E_n are equal to $R_{\rm Na}/(n-\delta)^2$, where $R_{\rm Na}=109\,734.6980$ cm^{-1} from the most recent [26] recommended value for R_∞ and the masses of the sodium atom and the electron. One expansion form for the QD parameter δ, a function of n for a given ^2L_J manifold, is

$$\delta=a_0+a_1t+a_2t^2+a_3t^3+\cdots , \tag{1}$$

where t is the binding energy in rydbergs,

$$t=\frac{1}{(n-\delta)^2} . \tag{2}$$

For discrete n,L,J states, an iteration is required. Alternative expansion forms have been used to avoid this itera-

TABLE VI. Least-squares fit to optical, infrared, and microwave data on sodium ^2S states to obtain QD parameters.

Interval n_1	Interval n_2	Experimental data	Observed −fitted	Expt. uncert.	Ref.
3	4	25739.988[a]	0.0006[a]	0.010[a]	[12]
3	5	33200.672[a]	−0.0003[a]	0.002[a]	[13,14]
3	6	36372.617[a]	0.0006[a]	0.002[a]	[13,14]
3	7	38012.041[a]	0.0002[a]	0.002[a]	[13,14]
3	8	38968.51[a]	0.002[a]	0.02[a]	[12]
3	9	39574.84[a]	−0.008[a]	0.02[a]	[12]
3	10	39983.26[a]	−0.002[a]	0.02[a]	[12]
3	11	40271.37[a]	−0.026[a]	0.02[a]	[12]
3	12	40482.22[a]	−0.016[a]	0.02[a]	[12]
11	∞	1178.0555[a]	0.00011[a]	0.0015[a]	d
12	∞	967.2151[a]	−0.00011[a]	0.0004[a]	d
32	33	217.752809[b]	−0.45[c]	9[c]	[8]
33	34	198.053956[b]	−1.51[c]	12[c]	[8]
34	35	180.661460[b]	4.09[c]	7[c]	[8]
36	37	151.538237[b]	2.94	6[c]	[8]
39	40	118.520443[b]	−4.03[c]	4[c]	[8]
40	41	109.666928[b]	0.35[c]	4[c]	[8]

[a]Values in cm^{-1}.
[b]Values in GHz.
[c]Values in kHz.
[d]This work.

tion. They may be written

$$\delta = a_0 + a_1 u + a_2 u^2 + a_3 u^3 + \cdots , \quad (3)$$

where

$$u = \frac{1}{(n-\delta_0)^2} . \quad (4)$$

Martin [4] has used $\delta_0 = 1.4$ for the ^2S states and $\delta_0 = 0$ for the ^2D states. Others [6–8,11] have used the form (3) with $\delta_0 = a_0$.

Present and previously published values for the QD parameters are given in Table VII. In cases for which the δ_0 parameter is omitted, the expansion form (1) was used. We find that when form (3) is used, the higher-order terms in the expansion are quite sensitive to the assumed value of δ_0. The variance of the global fit (rms ratio of discrepancy to estimated experimental error) was 0.33 when expression (1) was used, or when (3) was used with $\delta_0 = 1.35$ or $\delta_0 = a_0$, but increased to 1.1 when $\delta_0 = 1.4$. In the following, we use the form (3) with $\delta_0 = a_0$ to avoid an extra parameter and to obtain smaller variances.

Results of a fit to sodium ^2D-state levels are also given in Table VII. The ^2D-state fine-structure splitting has been measured over the range $n = 3$–31 by a variety of techniques [14,24,27,28]. Our fitted difference of QD parameters for the two fine-structure parameters, given in Table VII, was used in the Stark-level-structure calculations discussed above. Quantum-defect parameters for sodium ^2P states and for $L \geq 3$ are given in Sec. VI.

V. IONIZATION ENERGY OF NEUTRAL SODIUM

One useful feature of the electric-field-scan data is that the comparison with computed Stark levels yields the binding energy (energy difference with respect to ionization) of the upper-state levels, rather than the difference between two quantum levels, as in most spectroscopic work. We now show that an improved value for the ionization limit of the sodium ground state can be obtained from the upper-state binding energies by adding four accurately known intervals. Three of these intervals are obtained from previous measurements, while the fourth is determined from fitted parameters. Table VIII, in conjunction with previously presented results, summarizes this analysis, while Fig. 6 shows the relevant intervals on a NaI term diagram.

The excitation energies of the $n = 11$ and $12\,^2S$ states are obtained in three steps. The sodium D lines have been measured to 2.5 parts in 10^9, or about 4×10^{-5} cm^{-1} by Juncar *et al.* [13]. For the $D1$ line, their reported value is equal to 16 956.170 25(4) cm^{-1}, and the $D2$ line is 16 973.366 19(5) cm^{-1}. Measurements of the 11 or $12\,^2S$–$3\,^2P$ interval are only reliable to about 0.02 cm^{-1} and hence inadequate for our purposes. Hence, for this interval, we use the sum of interferometric measurements [14] and fitted values. The Meissner and Luft [14] measured intervals for $n\,^2S$ or $3\,^2P$, where $n = 5$, 6, and 7, with adjustments for the Kr standard [25] and error limits as discussed above, are shown in Table VIII, lines 1 and 2.

The remaining interval, from 5, 6, or $7\,^2S$ to 11 or $12\,^2S$ is determined from the global fit of QD parameters to all sodium ^2S Rydberg levels. These particular intervals are obtained with high accuracy because they amount to interpolations between larger intervals between lower-n levels from interferometric data and smaller intervals between higher-n levels from microwave data. When the uncertainties in the quantum-defect parameters are propagated appropriately, we find that the intervals from $5\,^2S$ to 11 or $12\,^2S$ have uncertainties of 2×10^{-3} cm^{-1}, while the intervals from 6 and $7\,^2S$ are known to better than 1×10^{-3} cm^{-1}. In fitting the data to QD parameters, only energy differences were used for all but the 11 and $12\,^2S$ states, so that the ionization energy itself does not enter, although numerically this can be obtained from the QD of the $3\,^2S$ state. Of course, this fitting procedure does assume the constraint of a four-term expansion for the QD parameters, and hence assumes a smooth variation with energy. The previous determination of the ionization energy by Risberg [12], reviewed by Martin [4],

TABLE VII. QD parameters for sodium ^2S and ^2D states compared with previously quoted values. The expansion parameters are defined in Eqs. (1)–(4) in the text. The difference of the quantum defects for $^2D_{5/2}$ and $^2D_{3/2}$ (last line) has been obtained by least-squares fits to all the available data.

State	δ_0	a_0	a_1	a_2	a_3	Ref.
^2S		1.3479506	0.061369	0.015852	−0.009033	[12]
^2S	a_0	1.3479692(4)	0.06137(10)			[8]
^2S	1.4	1.3479644	0.0601426	0.006956	0.006493	[4](1)
^2S	1.4	1.3479714	0.0599735	0.008050	0.0004683	[4](2)
^2S	a_0	1.347964	0.060673	0.0233	−0.0085	[7]
^2S	a_0	1.34796938	0.0609892	0.0196743	−0.001045	a
		±0.00000011	±0.0000164	±0.00001726	±0.000354	
^2D		0.0148972	−0.042146	0.006323		[12]
^2D	0	0.0149013	−0.042472	0.006401		[4]
^2D	a_0	0.015543	−0.08535	0.7958	−4.0513	[7]
^2D	a_0	0.0149084(17)	−0.042366(57)	0.00859(40)		a
$^2D^{b}_{dif}$		$1.483(5)\times10^{-5}$	$-7.809(11)\times10^{-5}$			[14,24,27,28]

[a]This work.

[b]$\delta(^2D_{5/2}) - \delta(^2D_{3/2})$.

TABLE VIII. Data used to derive a new value for the ionization energy of neutral sodium. The first two lines give the data of Ref. [14] corrected as proposed in Ref. [25]. Line 3 gives the $n\,^2S$-term energy obtained from the above data and the D line data of Ref. [13]. Lines 4 and 5 give the $11\,^2S-n\,^2S$ and $12\,^2S-n\,^2S$ intervals, respectively, as obtained from the fitted QD parameters given in Table VII. Lines 6 and 7 give the $11\,^2S$- and $12\,^2S$-term energies obtained from lines 3 and 4 or 5, respectively. The eighth and ninth lines give the ionization energy computed from the sums of figures in lines 3 and 4 or 5, and the experimental binding energies given in Table V.

Intermediate state	$n=5$ (cm^{-1})	$n=6$ (cm^{-1})	$n=7$ (cm^{-1})
$n\,^2S-3\,^2P_{3/2}$	16227.306(2)	19399.251(2)	21038.675(2)
$n\,^2S-3\,^2P_{1/2}$	16244.502(2)	19416.447(2)	21055.870(2)
$E(n\,^2S)$	33200.672(2)	36372.617(2)	38012.041(2)
$E(11\,^2S)-E(n\,^2S)$	7070.723(2)	3898.779(1)	2259.355(1)
$E(12\,^2S)-E(n\,^2S)$	7281.564(2)	4109.619(1)	2470.195(1)
$E(11\,^2S)$	40271.395(3)	40271.396(2)	40271.396(2)
$E(12\,^2S)$	30482.236(3)	40482.236(2)	40482.236(2)
E_{ion}(via $11\,^2S$ and $n\,^2S$)	41449.451(3)	41449.452(2)	41449.452(2)
E_{ion}(via $12\,^2S$ and $n\,^2S$)	41449.451(3)	41449.451(2)	41449.451(2)
E_{ion}(average)		41449.451(2)	
E_{ion}(previous[a])		41449.44(3)	

[a]Reference [12].

was somewhat more dependent on the QD expansion because it was necessary to extrapolate from the highest observed levels to the series limit, whereas in our analysis it is only necessary to extrapolate up to 11 or $12\,^2S$.

The value we obtain for the ionization energy of sodium, 41 449.451(2) cm^{-1}, applies to the mean of the hyperfine levels of the $3\,^2S$ ground state. It is well within

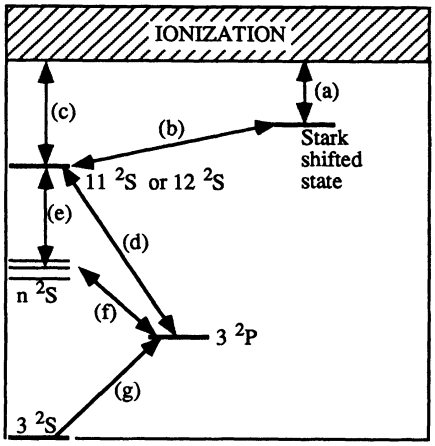

FIG. 6. Level diagram of sodium (not to scale) showing energy intervals discussed in the text, some of which are used to obtain the improved value of the ionization energy of ground-state sodium. (a) Fitted Stark-shifted binding energy determined in this work. (b) CO_2-laser photon energy. (c) The $11\,^2S$ or $12\,^2S$ binding energy determined from (a) and (b) as described in the text. (d) $11\,^2S$ or $12\,^2S-3\,^2P$ intervals known only to about 0.02 cm^{-1} and therefore not used in the computation of the improved value of the ionization energy. (e) $11\,^2S$ or $12\,^2S-n\,^2S$ ($n=5-7$) intervals determined from global fits to all sodium $n\,^2S$ Rydberg levels as described in the text. (f) $n\,^2S-3\,^2P$ ($n=5-7$)intervals [14]. The intervals (e) and (f) made it possible to circumvent using the interval (d). (g) The $3\,^2P-3\,^2S$ intervals, the sodium D lines [13].

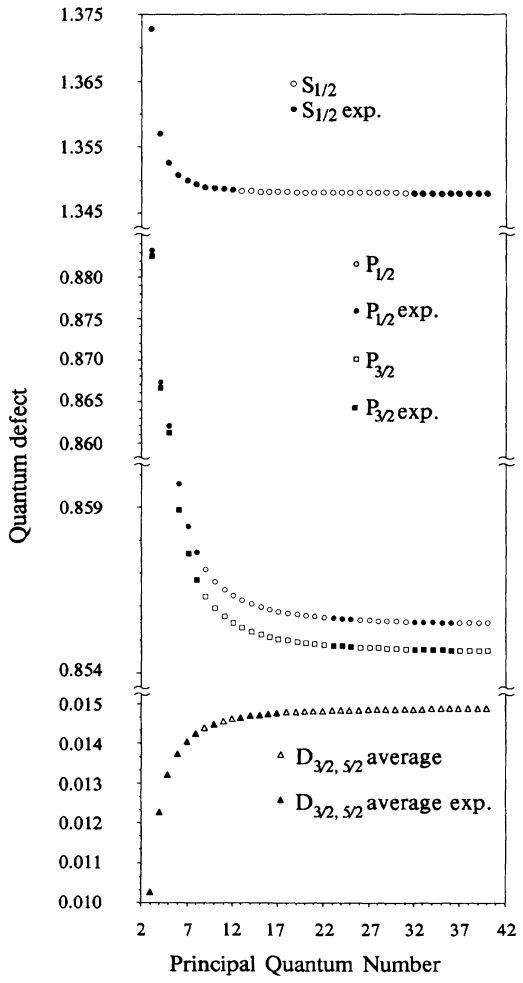

FIG. 7. Quantum defects vs n for sodium $^2S_{1/2}$, $^2P_{1/2}$, $^2P_{3/2}$, and ^2D states. The filled diamonds, squares, etc., are used for levels for which optical or MW data exist while open symbols represent fitted values.

TABLE IX. Data on sodium ^2P states showing the quality of fits to QD parameters. In the second and sixth columns, the experimental data are stated in terms of a QD for each n level, with error limits σ given in the third and seventh columns. The discrepancies resulting from fits with four and five parameters are given in columns 4, 5, 8, and 9. In computing the δ_n values, we used $R_{Na}=109\,734.698$ cm^{-1}, E_{ion} from Table VIII, together with data from Ref. [13] ($n=3$), Ref. [12,29] ($n=4$–8), and Ref. [11] ($n=23$–36).

	$^2P_{1/2}$		10^6(Expt.−fit)		$^2P_{3/2}$		10^6 (Expt.−fit)	
n	δ_n (Expt.)	$10^6\sigma$ (Expt).	4 par	5 par	δ_n (Expt.)	$10^6\sigma$ (Expt.)	4 par	5 par
3	0.8833527	0.1	0.0	0.0	0.8826093	0.1	0.0	0.0
4	0.8674105	1.4	0.2	0.0	0.8666274	1.4	0.3	0.0
5	0.8621532	6.5	−10.5	4.7	0.8613556	6.5	−15.3	4.6
6	0.8597520	19.0	−6.3	−38.8	0.8589530	19.0	−5.9	−38.5
7	0.8584240	32.0	−26.7	−77.7	0.8576320	32.0	−14.8	−68.4
8	0.8576440	50.0	−15.9	−69.0	0.8568310	50.0	−21.9	−78.5
23	0.8556721	0.8	2.1	0.5	0.8548557	1.2	3.5	−0.2
24	0.8556522	0.9	1.6	1.0	0.8548359	0.6	2.6	0.7
25	0.8556300	2.8	−3.6	−3.2	0.8548169	1.3	0.1	−0.2
32	0.8555400	29.0	−16.0	−11.9	0.8547327	7.3	−6.8	−2.4
33	0.8555279	3.0	−6.7	−1.6	0.8547273	2.0	−5.0	−0.2
34	0.8555302	8.3	−12.9	−7.4	0.8547142	5.5	−11.6	−7.4
35	0.8555279	1.8	−9.3	−3.4	0.8547131	1.8	−6.8	−1.2
36	0.8555254	3.0	−7.0	−0.1	0.8547061	1.8	−8.0	−2.4

the error limits of the previous value, quoted by Risberg [12] and Martin [4] of 41 449.44(3) cm^{-1}.

VI. QD PARAMETERS FOR SODIUM ^2P STATES AND FOR $L \geq 3$

The above value for the ionization energy, together with MW[11] and interferometric [13] data obtained since 1980, leads to a slight revision of the ^2P-state QD parameters. A survey of the data and fit results for the ^2P manifolds of sodium reveals significant gaps as well as inconsistencies at a certain level of precision. The overall trend of the QD parameters $\delta(L,n)$ is shown in Fig. 7. More detailed fit results are presented in Tables IX and X and in Fig. 8.

Table IX shows input data stated in terms of QD parameters $\delta_n = n - \sqrt{R_{NA}/(E_{ion}-E_n)}$. The error limits are propagated from uncertainties in E_{ion} and in the experimental transition frequencies. Thus $\sigma(\delta_n)=\sigma(n^*)=n^*\sigma(T_n)/2T_n$, where $\sigma(y)$ denotes the standard deviation of the quantity y, and $T_n = E_{ion}-E_n$. The same data are plotted in Fig. 8. To expand the scale for this figure, we have subtracted values calculated from the three-parameter fits.

The data for $n=3$–8 were obtained using optical and interferometric techniques [12–14,29]. To obtain δ_n values, E_{ion} from Table VIII was used. For $N=23$–36 the original [11] $^2S \leftrightarrow {}^2P$ MW transitions are used with ^2S quantum defects recalculated from the fit results of Sec. IV. (Differences in δ_n with values given in Ref. [11] are negligible for $n \geq 32$, and less than one standard deviation in every case.) Table IX and Fig. 8 show that for the determination of δ_n, the MW and interferometric data ($n=3$ and 4) are of comparably good quality, but over the range $5 \geq n \geq 22$, the data are inferior or lacking.

When fitted separately, the MW and the optical data lead to incompatible QD expansion parameters. We find that the difference between the MW and optical values for a_0 is more than 4(6) times the sum of standard deviations from the two fits for the $^2P_{1/2}$ ($^2P_{3/2}$) manifold. When the MW and optical data are combined in a weighted least-squares fit, five parameter fits do reproduce the data to a standard deviation of less than 2, where the standard deviation of a fit to N data points, T_i, is taken as

$$\sigma = \left[\sum_i^N \frac{(T_{i,\text{obs}} - T_{i,\text{calc}})^2}{(N-c)\sigma_i^2} \right]^{1/2}, \tag{5}$$

TABLE X. QD parameters for sodium ^2P, for which results from the 3, 4, and 5 parameter fits are given, and ^2F states. The column labeled σ gives the standard deviation of the fit. The expansion form (3) with $\delta_0=a_0$ is used. (Digits beyond the uncertainty limits are given so as to reproduce the input data.)

State	σ	a_0	a_1	a_2	a_3	a_4
$^2P_{1/2}(3)$	3.1	0.85544557	0.1096151	0.086155		
$^2P_{1/2}(4)$	2.2	0.85544081	0.1122869	0.047895	0.119926	
$^2P_{1/2}(5)$	1.4	0.85542918	0.1192484	−0.178762	2.279752	−5.81095
$^2P_{3/2}(3)$	3.5	0.85462791	0.1099854	0.086540		
$^2P_{3/2}(4)$	2.6	0.85462299	0.1129312	0.044272	0.132633	
$^2P_{3/2}(5)$	1.3	0.85461115	0.1204065	−0.203076	2.509007	−6.42113
^2F	1.7	0.00162200	−0.0051628	−0.025644		

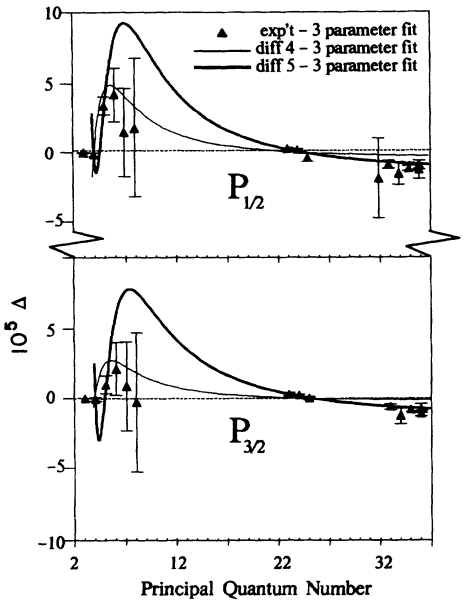

FIG. 8. Differences between values from three-parameter fits for sodium $^2P_{1/2}$ (top) and $^2P_{3/2}$ (bottom) state quantum-defect parameters, times 10^5, and (a) experimental data (triangles and error bars), (b) four-parameter fit results (light solid line), and (c) five-parameter fit results (heavy solid line). The results of three-parameter fits are subtracted out in order to expand the scale. A fit with five parameters is needed to come within error limits of both the MW results ($n=23$–36) [11] and the values for $n=3$ and 4, which are based on the value of $E_{\rm ion}$ from Table VIII and interferometric and optical data [12–14].

where σ_i is the experimental standard deviation of level i, and c is the number of fitted parameters. At a level of 10^{-5}, however, the interpolated values for intermediate n vary considerably depending on whether 3, 4, or 5 QD expansion parameters are fitted. In Tables IX and X, we present results from fits to the $^2P_{1/2}$ and $^2P_{3/2}$ data with both four and five parameters. With four parameters, the microwave measurement for $n=35$ differs from the fitted value by more than five standard deviations, showing again the incompatibility of the MW and optical data. For many purposes, including Stark-structure calculations here, the disagreement is too small to be significant. However, spectroscopic measurements on $n=10$–12 ^2P states of the kind reported here for $n=10$–12 ^2S and ^2D states would yield error limits as low as 0.5×10^{-5}, hence they help considerably to remove the ambiguity in interpolating the fit results to intermediate n values.

Discrepancies between MW and optical QD parameters have been noted with regard to the $^2D_{5/2}$ manifold of Cs [6], and the question of possible Stark shifts in the MW data was raised. However, for sodium ^2P manifolds, in the absence of data on the same n level by different methods, or on intermediate N levels, there is no reason to reject any of the optical or MW data presently available on sodium The relatively rapid variation of δ_n for sodium $n=3$–6 ^2P states, leading to diverging coefficients in the QD expansion, is also similar to the situation in Cs $^2D_{5/2}$ states [6].

For Na ^2F states, we have also performed a fit to combined MW [9] and optical [14,12,29] data, with results as shown in Table X for the center of gravity of the ^2F terms. The fine-structure splitting has been found to be very nearly hydrogenic [9]. From the Dirac formula, one obtains the fine-structure splitting in level n,L that corresponds to a quantum-defect difference $\delta(^2L_{J=L-1/2})-\delta(^2L_{J=L+1/2})=\alpha^2/2L\,(L+1)$. Hence $\alpha^2/42=1.27\times10^{-6}$ should be added to the QD parameter a_0 for $^2F_{5/2}$ and $\alpha^2/56=9.51\times10^{-7}$ should be subtracted from a_0 for $^2F_{7/2}$.

For $L\geq4$, as discussed by Freeman and Kleppner [23], the dipole-polarizability term dominates the quantum-defect expansion, and there is also a small contribution from the quadrupole polarizability and from relativistic effects. QD parameters for the center of gravity of the $L\geq4$ terms have been given in Refs. [23] and [4].

ACKNOWLEDGMENTS

The work at the University of Missouri–St. Louis was supported by National Science Foundation Grants No. PHY-8907698 and No. INT-8719649 and the University of Missouri Weldon Spring Fund. The authors would like to thank Philip H. Schmidt and Thomas E. Hezel for technical assistance and aid in the acquisition of data. The work at Stony Brook was supported by National Science Foundation Grant No. PHY-9012830 to H. J. Metcalf. Some of the calculations were performed with the facilities of the Cornell National Supercomputer Facility, which receives major funding from NSF and IBM.

[1] J. Stark, Ann. Phys. (Leipzig) **43**, 965 (1914); Berl. Ber. **47**, 932 (1913).
[2] A. Lo Surdo, Lincei Rend. **22**, 664 (1913); Cim. **7**, 335 (1914).
[3] M. L. Zimmerman, M. G. Littman, M. M. Kash, and D. Kleppner, Phys. Rev. A **20**, 2251 (1979).
[4] W. C. Martin, J. Opt. Soc. Am. **70**, 784 (1980).
[5] B. P. Stoicheff and E. Weinberger, Can. J. Phys. **57**, 2143 (1979).
[6] K.-H. Weber and C. J. Sansonetti, Phys. Rev. A **35**, 4650 (1987).
[7] C.-J. Lorenzen and K. Niemax, Phys. Scr. **27**, 300 (1983).
[8] P. Goy, C. Fabre, M. Gross, and S. Haroche, J. Phys. B **13**, L83 (1980).
[9] T. F. Gallagher, R. M. Hill, and S. A. Edelstein, Phys. Rev. A **14**, 744 (1976).
[10] C. Fabre, S. Haroche, and P. Goy, Phys. Rev. **18**, 229 (1978).
[11] C. Fabre, S. Haroche, and P. Goy, Phys. Rev. **22**, 778 (1980).
[12] P. Risberg, Ark. Fys. **10**, 583 (1956).
[13] P. Juncar, J. Pinard, J. Hamon, and A. Chartier, Metrologia **17**, 77 (1981). We thank W. C. Martin for directing us to this reference.
[14] K. W. Meissner and K. F. Luft, Ann. Phys. (Liepzig) **29** (5), 698 (1937).

[15] C. E. Burkhardt, M. Ciocca, J. J. Leventhal, E. Arimondo, T. Bergeman, and S. T. Manson, Nucl. Instrum. Methods Phys. Res. **B56/57**, 313 (1991).
[16] C. E. Burkhardt, J. L. Libbert, J. Xu, J. J. Leventhal, and J. D. Kelley, Phys. Rev. A **38**, 5949 (1988).
[17] P. McNicholl, T. Bergeman, and H. J. Metcalf, Phys. Rev. A **37**, 3302 (1988).
[18] D.-H. Yang, D. Lieberman, P. van der Straten, T. Bergeman, and H. J. Metcalf, Phys. Rev. A **40**, 5026 (1989).
[19] L. C. Bradley, K. L. Soohoo, and C. Freed, IEEE J. Quantum Electron **22**, 234 (1986).
[20] W. J. Witteman, *The CO_2 Laser* (Springer-Verlag, New York, 1987).
[21] H. W. Mocker, Appl. Phys. Lett. **12**, 20 (1968). We acknowledge P. M. Koch for directing us to this reference.
[22] S. A. Bhatti, C. L. Cromer, and W. E. Cooke, Phys. Rev. A **24**, 161 (1981).
[23] R. R. Freeman and D. Kleppner, Phys. Rev. A **14**, 1614 (1976).
[24] C. Fabre, M. Gross, and S. Haroche, Opt. Commun. **13**, 393 (1975).
[25] W. C. Martin and R. Zalubas, J. Phys. Chem. Rev. Data **10**, 153 (1981).
[26] B. N. Taylor and E. R. Cohen, J. Res. NIST **95**, 497 (1990).
[27] K. Fredriksson and S. Svanberg, J. Phys. B **9**, 1237 (1976).
[28] G. Leuchs and H. Walther, Z. Phys. A **293**, 93 (1979).
[29] I. Johansson, Ark. Fys. **20**, 135 (1961).

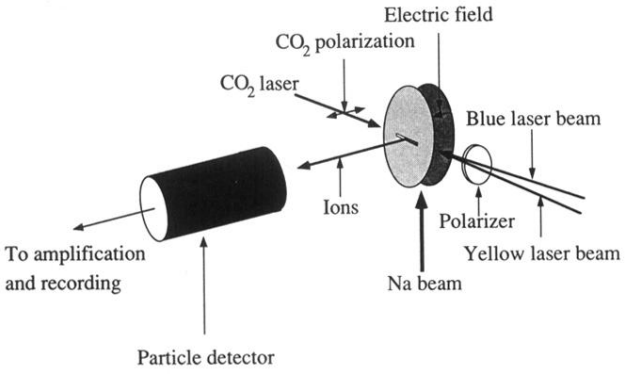

FIG. 2. Schematic diagram of the apparatus.